



Extracting vibration signal from measured data polluted by thermal noise using a Kalman filtering technique

Bin Wu (1), Kaichen Song (1) and Jie Pan (2)

(1) College of Biomedical Engineering & Instrument Science, Zhejiang University, Hangzhou, China, 310027

(2) Department of Mechanical Engineering, The University of Western Australia, 35 Stirling Highway, Crawley, WA, 6009

ABSTRACT

In practice, a measured vibration signal is often mixed with the inherent thermal noise existing in the measurement system. It is difficult to use traditional frequency-domain filtering techniques as the desired vibration signal and the unwanted thermal noise may have components in the same frequency band. In this research, a dual-sensor vibration measurement system and a Kalman filter based on a linear prediction model are developed to reduce the thermal noise in measured data. This paper presents a mathematical analysis of the linear-prediction-based Kalman filter and examines the effects of the prediction error and measurement error on the filtering performance. The results show that the linear-prediction-based Kalman filter can reduce the prediction error compared to the traditional random-walk model. The effect of unsteady measurement error on filtering performance is also investigated. A simulation example is used for illustration. The simulation result shows that the linear-prediction-based Kalman filter achieves a better anti-drift performance than the conventional low-pass filter, and the delay of the linear-prediction-based Kalman filter is smaller than that of the conventional low-pass filter.

1 INTRODUCTION

Vibration measurement data polluted by thermal noise always exhibit a problem of drift. This drift problem causes the measurement error to diverge, especially when the measurement result is obtained by integrating the sensor data, which is common in displacement measuring applications that use velocity or acceleration sensors. However, it is difficult to eliminate thermal noise using traditional frequency-domain filtering techniques as the noise band and the signal band usually overlap with each other. To reduce the thermal noise in measured data, in this paper, we present a dual-sensor-based method and the corresponding filter algorithm.

Using multiple sensors to extract a vibration signal from data mixed with thermal noise has been shown to be feasible (Twerdochlib, 1989). Typically, sensors of the same type are used in a multi-sensor vibration measuring system, which leads to nearly identical noise characteristics. However, for the sensors used in a multi-sensor measuring system, there is a trade-off between low drift quality and high dynamic performance. High dynamic sensors are often plagued by a drift problem, which is caused by thermal noise. For example, the piezoelectric sensors can detect changes in force up to several MHz (Tressler *et al.*, 1998). However, the drift of piezoelectric sensor reaches about 1 N/min according to the practical experience. Low drift sensors usually use the feedback technique. A proof mass is controlled at the balance position to measure accelerations. For example, a closed-loop MEMS sensor is reported to have achieved a 10 μg bias stability under warmup (Zwahlen *et al.*, 2012). However, for these kinds of sensors, the signal bandwidth is usually below 1 kHz. Therefore, this paper proposes to combine different types of sensors in a vibration measuring system, each with individual noise characteristics and an appropriate sampling rate. A high-sample-rate sensor can contribute to the dynamic performance of the measuring system and a low-sample-rate sensor is used to calibrate the drift of the high-sample-rate sensor. This more complicated situation requires a suitable algorithm to fuse the measurement data from different sensors.

There are various fusion algorithms used in the multi-sensor measuring field. Among them, the complementary filter is widely used because it requires less computation. However, it is produced by a simple analysis in the frequency domain and it does not consider any statistical description of the noise corrupting the signal (Higgins, 1975). The Kalman filter, which is mostly applied to integrated navigation systems, has received much attention from the multi-sensor measuring field over the last two decades (Hall and Llinas, 1997). The general multi-sensor optimal information-fusion decentralised Kalman filter with a two-layer fusion structure is studied for discrete-time

linear stochastic control systems with multiple sensors and correlated noises (Sun and Deng, 2004). A method of transforming multi-rate data to single-rate data for a multi-sensor system has been developed (Yan *et al.*, 2006).

This paper focuses on the dual-sensor vibration measuring system. One sensor works at a high sample rate to provide the dynamic performance but its output is more sensitive to the thermal noise, and the other sensor works at a low sample rate to achieve low drift quality. A Kalman filter algorithm based on a linear prediction model is proposed to combine the high-dynamic and low-drift characteristics. The relationship between the prediction error and sample rate is studied. In addition, the effect of unsteady measurement error is investigated. The simulation results show that the thermal noise is reduced in the Kalman filter output. In addition, our method has smaller delay than a traditional frequency-domain filter, which may be a useful characteristic when applied in a closed-loop control system.

2 DUAL-SENSOR VIBRATION MEASURING SYSTEM

A block diagram of the dual-sensor vibration measuring system is shown in Figure 1. It consists of the hardware and the algorithm. The hardware structure contains a low-sample-rate sensor such as an optical vibration sensor which is insensitive to temperature and a high-sample-rate sensor which provides the dynamic performance. To simplify the following algorithm, the low-sample-rate sensor and the high-sample-rate sensor are synchronised and fixed at a constant ratio. The ratio of the low sample rate to the high sample rate depends on the thermal noise in the high-sample-rate sensor, as it requires the low sample rate to be higher than the Nyquist frequency of the thermal noise. As the output drift caused by thermal noise changes over a period of seconds (or longer), this requirement can be met in most conditions. There is a possibility that the low sample rate may become lower than the signal frequency, which would cause an aliasing problem in frequency domain for the low-sample-rate channel. However, in time domain, the data measured by low-sample-rate sensor is not distorted. In the multi-rate to single-rate conversion process, this aliasing problem can be corrected as the high-sample-rate sensor obtains the essential information.

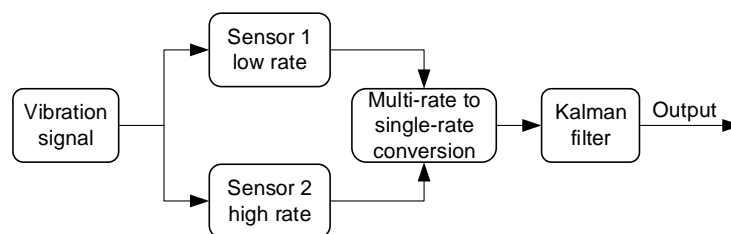


Figure 1: Block diagram of the hardware structure and the data fusion algorithm system.

In the multi-rate to single-rate conversion process, the low-sample-rate (Sensor 1) data and high-sample-rate (Sensor 2) data are processed to be interweaved, as shown in Figure 2. As the low sample rate and high sample rate are synchronised and kept at a constant ratio, a high-sample-rate datum will be substituted by the corresponding low-sample-rate datum every n high-sample-rate data. Here, n denotes the ratio of the high sample rate to the low sample rate. Since the data of Sensor 1 and Sensor 2 are interweaved, the signal bandwidth is decided by Sensor 2. When the signal frequency is higher than half of the sample rate of Sensor 1, the missing information in Sensor 1 is complemented by Sensor 2. The data measured by Sensor 1 cannot be distorted in time domain. Therefore, any anti-aliasing filter whose band is narrower than the signal band cannot be used before Sensor 1.

This processing method loses some information in the high-sample-rate data but simplifies the computation as the main operations in this process are counting and substitution. For signal processors in an embedded system, this simplification can save valuable computation time and memory space.

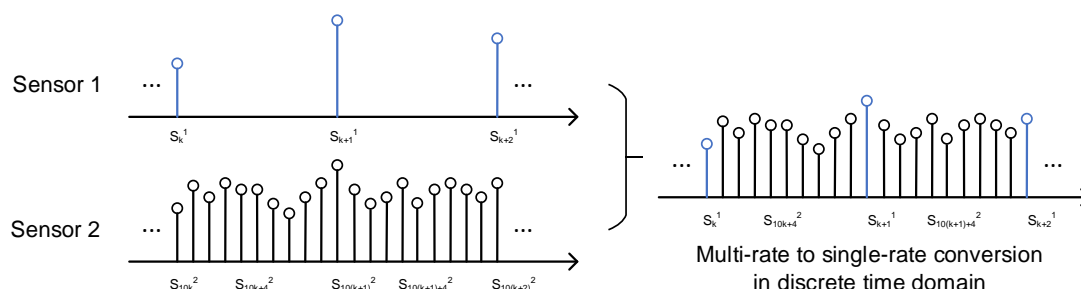


Figure 2: Illustration of the multi-rate to single-rate conversion process.

The converted single-rate data are then processed using the linear-prediction-based Kalman filter, which was developed from a random-walk forecast model. The random-walk forecast model assumes that the current state is equivalent to the last state. This assumption is reasonable when the data are sampled at a rate that is much faster than the dynamic of the state variable. The linear-prediction-based Kalman filter, as shown in Figure 3, was developed from a random-walk forecast model and assumes that the current data can be predicted by a linear fitting of several previous data. For example, for a fourth-order linear prediction model, the fifth datum is predicted by the four previous estimations. Each estimation is generated by the corresponding Kalman filter iteration. As new data comes in, the linear prediction model produces the new prediction value. Prior to the prediction value, the statistical characteristics of the prediction error are obtained according to the signal frequency and the sample rate of the single-rate data. Considering the prediction error and measurement error, the prediction value and measurement data are combined to generate the iteration result of the Kalman filter.

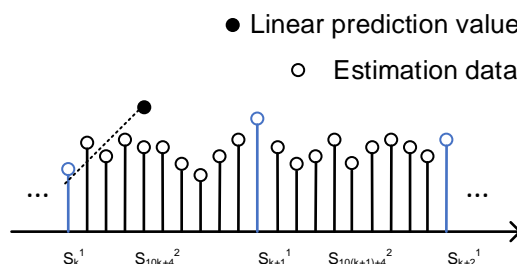


Figure 3: The linear prediction model applied to single-rate data.

The implementation of the Kalman filter is standard. As the core of the Kalman filter, the state variable x_n of the Kalman filter is given by:

$$x_n = [s_n \ s_{n-1} \ \dots \ s_{n-p}]^T, \quad (1)$$

where s_n is the n th state variable of the converted single-rate data and p is the order of the linear fitting equation. The state transmission equation can be expressed as:

$$\begin{bmatrix} s_n \\ s_{n-1} \\ \vdots \\ s_{n-p} \end{bmatrix} = \begin{bmatrix} c_1 & c_2 & \dots & c_p \\ 1 & 0 & \dots & 0 \\ 0 & 1 & \dots & 0 \\ \vdots & \vdots & \ddots & \vdots \\ 0 & 0 & \dots & 0 \end{bmatrix} \begin{bmatrix} s_{n-1} \\ s_{n-2} \\ \vdots \\ s_{n-(p+1)} \end{bmatrix}, \quad (2)$$

where c_p is the linear fitting coefficient. In a simpler form, the state transmission equation can also be expressed as:

$$x_{n|n-1} = F_n x_{n-1}, \quad (3)$$

where F_n is the state transmission matrix. Hence, the covariance matrix $\Sigma_{x_{n|n-1}}$ can be obtained by:

$$\Sigma_{x_n|n-1} = \Sigma_{\epsilon_n} + F_{n-1}\Sigma_{x_{n-1}}F_{n-1}^T, \quad (4)$$

where Σ_{ϵ_n} and $\Sigma_{x_{n-1}}$ are the covariance matrix of the prediction error and the last Kalman estimation, respectively. Based on the covariance matrix $\Sigma_{x_n|n-1}$, the gain factor is given by:

$$K_n = \Sigma_{x_n|n-1}A_n^T \left(\Sigma_{e_n} + A_n\Sigma_{x_n|n-1}A_n^T \right)^{-1}, \quad (5)$$

where A_n is the measurement matrix and Σ_{e_n} is the covariance matrix of the measurement error. The measurement matrix converts the state variable into an observable vector. In this paper, the state variable is measured directly, hence the measurement matrix is an identity matrix. The covariance matrix of the measurement error is affected by the new arriving data as the data from different sensors have different noise characteristics. The estimation given by the Kalman filter can be expressed as:

$$x_n = x_n|n-1 + K_n(b_n - A_n x_n|n-1), \quad (6)$$

where b_n is the measurement vector. Each measurement vector is extracted from the single-rate data series and has the same dimension as the state variable. The difference between the measurement and prediction values is amplified by the Kalman gain, which is used to correct the prediction value and then generate the new estimation. The covariance matrix of the new estimation is given by:

$$\Sigma_{x_n} = (I - K_n A_n)\Sigma_{x_n|n-1}. \quad (7)$$

3 STUDY OF PREDICTION ERROR AND MEASUREMENT ERROR

The covariance matrix of the prediction error is influenced by three factors: the order of the linear prediction model, the signal frequency, and the sample rate of the single-rate data. For a p -order linear prediction model, each state variable s_n is a combination of p previous state variables and the q^{th} combination coefficient can be expressed as:

$$c_q = \left(\frac{6}{-p^2+p} - \frac{12(p+1)}{-p^3+p} \right) (p+1-q) + \frac{6(p+1)}{-p^2+p} - \frac{2(2p+1)}{-p^2+p}, q \geq 2. \quad (8)$$

As the true previous states are unavailable, the previous Kalman filter estimations are used to generate the new prediction. In theory, different estimations have different variances and should be assigned different weights. However, this requires us to change the state transmission matrix during each updating step, which increases the complexity of the algorithm. Here, the coefficient c_q is obtained under the assumption that each estimation has the same variance.

The simplest model is a random-walk model, which has only one coefficient, c_1 . To achieve a sufficiently small prediction error, the random-walk model has a high requirement for the ratio of the sample rate to the signal frequency. The solution to this problem is increasing the order of the prediction model. A simulation result indicating the relationship between the prediction error and the model order is shown in Table 1. In this table, the sample rate is fixed at 10 kHz and the signal is a band-limited random signal, with its highest frequency below 10 Hz and its amplitude normalised as 1. The second-order linear prediction model greatly improved the prediction error compared to the random-walk model. For a higher-order linear prediction model, the prediction error is not reduced but instead is increased. This can be explained by the transfer function of linear-prediction model. This model is equivalent to a low pass filter. The error is decided by gain of the transfer function in interested frequency band. Since the signal frequency is below 10 Hz in this simulation, the investigation on ultra-low frequency band shows that the second-order model has smaller prediction errors than higher orders. Considering the additional computational load when the model order becomes higher, the optimal choice is to use a second-order linear prediction model for signals below 10 Hz.

Table 1: The effect of the model order on prediction error.

Order	Standard deviation
1	1.3e-3
2	7.6e-6
4	2.2e-5
10	1.1e-4

When the band of the signal is broadened, the prediction errors of all models also increase if the sample rate remains the same. The reason is that the prediction value cannot follow the high-frequency component in the vibration signal. When the prediction error becomes as big as the measurement error, it will degrade the performance of the Kalman filter.

In the case of dual sensor fusion, the measurement error is unsteady. In the measurement vector b , the component b_i may be generated by the low-sample-rate sensor or the high-sample-rate sensor. The corresponding covariance matrix Σ_{e_n} thus changes during each measurement-updating step. As the low-sample-rate sensor has better noise performance, it will be assigned more weight during the estimation-updating step. The Kalman filter output is corrected each time a new low sample rate is obtained.

4 SIMULATION

To demonstrate the validity of the linear-prediction-based Kalman filter, this paper simulates a dual-sensor measuring system, as shown in Figure 4. In the simulation, sensor 1 is the low-sample-rate sensor and sensor 2 is the high-sample-rate sensor, whose sample rates are 200 Hz and 10 kHz, respectively. Corresponding to the different sample rates, these two sensors have different noise characteristics. The data of sensor 1 are polluted by a band-limited white noise whose standard deviation is 0.01, while the data of sensor 2 are polluted by a band-limited white noise and a thermal noise. The standard deviation of the white noise in sensor 2 is 0.1. The thermal noise has an effect on output drift. The output drift of sensor 2, written n_t , is designed to be a polynomial function of time as shown in Equation 9. Both the white noise and the output drift are additive.

$$n_t = 1 \times 10^{-1} \times t + 3 \times 10^{-2} \times t^2 + 6 \times 10^{-3} \times t^3 + 9 \times 10^{-4} \times t^4. \quad (9)$$

For clarity, the frequency of the original signal is limited below 10 Hz. The amplitude of the original signal is normalised as 1. The data of sensor 1 are equivalent to the sum of the original signal and the relatively smaller white noise. The curve of sensor 1 shows that the measurement data do not include any drift. The data of sensor 2 are equivalent to the sum of the original signal, the relatively bigger white noise and the output drift. The curve of sensor 2 shows that the measurement data include more noise and a time-varying drift.

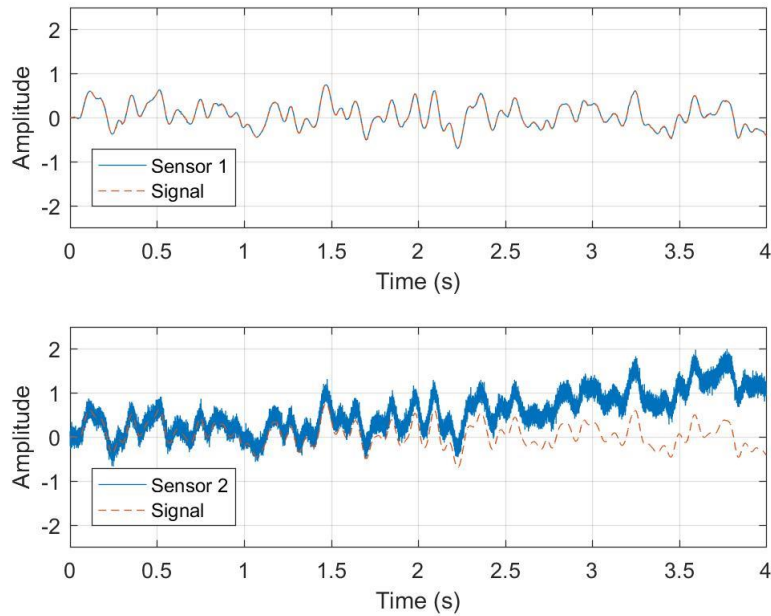


Figure 4: Simulation of low-sample-rate data and high-sample-rate data.

The two sources of data are inputted to the rate-converting module to produce the single-rate data. As the ratio of the high sample rate to the low sample rate is 50, then every fifty data points of sensor 2 there is one point substituted by a sensor 1 data point. The associated measurement variance is also substituted corresponding to the measurement data. The variance of sensor 1 is $1e-4$ and the variance of sensor 2 is 0.19. The variance of sensor 2 is fixed as a constant value. This may not be the optimal solution to the time-varying drift problem.

The simulation result is presented in Figure 5. Firstly, a traditional low-pass filter designed in the frequency domain is directly applied to the data of sensor 2. Our simulation shows that the high-frequency noise can be removed but the output drift caused by thermal noise cannot be cancelled. Secondly, the data of sensor 1 and sensor 2 are processed by the linear-prediction-based Kalman filter. The simulation result shows that the output drift can be reduced and the high-frequency noise can be improved. In addition, the latency of the low-pass filter is 179 samples while the latency of the Kalman filter is 0.

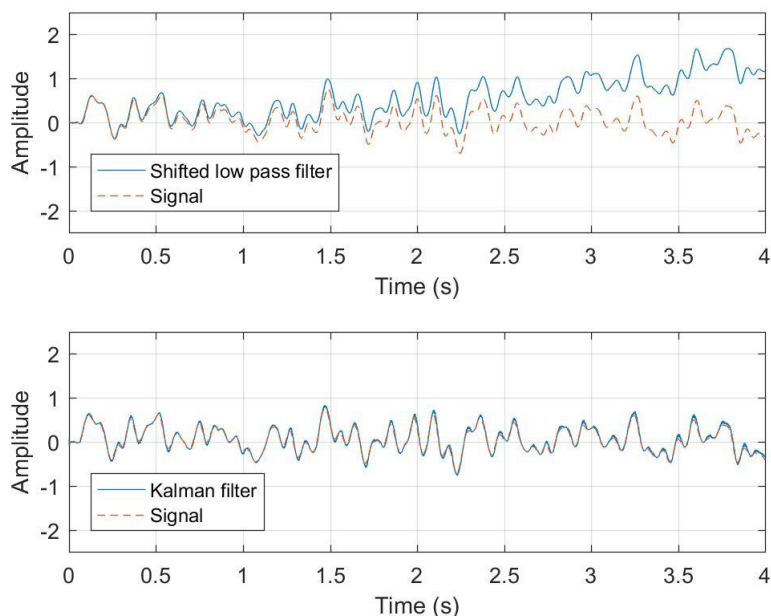


Figure 5: Simulation of the low-pass filter and the linear-prediction-based Kalman filter.

The power spectrums of the errors of these two algorithms are shown in Figure 6. Our analysis shows that the Kalman filter helps to reduce the error by 31 dB in the low-frequency band compared to the direct low-pass filter. However, in the mid- and high-frequency bands, the error of the linear-prediction-based Kalman filter is relatively larger than that of the low-pass filter. This is caused by the gap between the low-sample-rate data and the high-sample-rate data. A triangular wave appears in the later output of the Kalman filter.

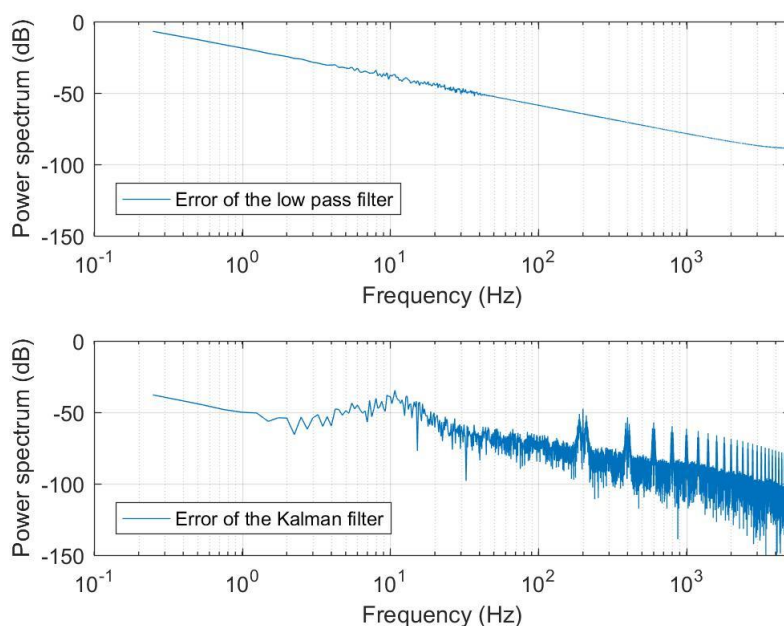


Figure 6: Power spectrums of the errors of the two different algorithms.

As the range of the signal frequency becomes wider, the anti-drift performance of the Kalman filter tends to become poorer. The improvements of the Kalman filter compared to the low-pass filter in the low-frequency band are shown in Table 2. The reason is that as the amplitude of the triangular wave becomes larger, the output error of the Kalman filter is increased.

Table 2: Anti-drift improvement of the Kalman filter for signals with different frequency ranges.

Frequency (Hz)	Improvement (dB)
10	31
50	12
100	5

5 CONCLUSIONS

This paper presented a dual-sensor-based measuring system and a corresponding Kalman filter algorithm to provide high-dynamic and low-drift vibration measuring ability. The simulation results verified its feasibility. However, there is still room for improvement in the algorithm. The measurement variance of the high-sample-rate sensor should be adjusted as the temperature changes rather than be fixed at a constant value. We have confidence that this improvement can eliminate the triangular wave in the output of the Kalman filter, which has the benefit of reducing high-frequency noise and enhancing anti-drift improvement for signals with broader frequency range.

ACKNOWLEDGEMENTS

This research was supported by the International Cooperation and Exchange Foundation for Doctoral Students of Zhejiang University.

REFERENCES

- Hall, D.L., and J. Llinas. 1997. "An Introduction To Multisensor Data Fusion". *Proceedings Of The IEEE* 85 (1): 6-23. doi:10.1109/5.554205.
- Higgins, Walter. 1975. "A Comparison Of Complementary And Kalman Filtering". *IEEE Transactions On Aerospace And Electronic Systems* AES-11 (3): 321-325. doi:10.1109/taes.1975.308081.
- Sun, Shu-Li, and Zi-Li Deng. 2004. "Multi-Sensor Optimal Information Fusion Kalman Filter". *Automatica* 40 (6): 1017-1023. doi:10.1016/j.automatica.2004.01.014.
- Tressler, J. F., S. Alkoy, and R. E. Newnham. 1998. "Piezoelectric Sensors And Sensor Materials". *Journal Of Electroceramics* 2 (4): 257-272.
- Twerdochlib, Michael. 1989. "Method For Eliminating Sensor Drift In A Vibration Monitoring System". *The Journal Of The Acoustical Society Of America* 86 (2): 857-857. doi:10.1121/1.398756.
- Yan, L.P., B.S. Liu, and D.H. Zhou. 2006. "The Modeling And Estimation Of Asynchronous Multirate Multisensor Dynamic Systems". *Aerospace Science And Technology* 10 (1): 63-71. doi:10.1016/j.ast.2005.09.001.
- Zwahlen, P., Y Dong, A. M. Nguyen, F. Rudolf, J. M. Stauffer, P. Ullah and V. Ragot. 2012. "Breakthrough in high performance inertial navigation grade Sigma-Delta MEMS accelerometer". In *Position Location and Navigation Symposium (PLANS), 2012 IEEE/ION* (pp. 15-19). IEEE.